Characterization of electromagnetic pulses via arrays on ShenGuang-III laser facility laser

Ming Yang (杨 鸣)[1], Tingshuai Li (李廷帅)[1], Chuanke Wang (王传珂)[2], Jinwen Yang (杨进文)[1,2], Weiming Yang (杨为明)[2], Tao Yi (易 涛)[2,*], Shenye Liu (刘慎业)[2], Shaoen Jiang (江少恩)[2], and Yongkun Ding (丁永坤)[2]

[1]*School of Energy Science and Engineering, University of Electronic Science and Technology of China, Chengdu 611731, China*

[2]*Laser Fusion Research Center, Chinese Academy of Engineering Physics, Mianyang 621900, China*

**Corresponding author: yitao2008@caep.cn*

Received June 8, 2016; accepted August 12, 2016; posted online September 13, 2016

Intensive electromagnetic pulses (EMPs) can be generated from interaction of the ultra-intense lasers and solid targets in inertial confinement fusion (ICF), which will detrimentally affect the data acquisition from some electric components. A diagnostic system for EMP measurement inside and outside the ShenGuang-III facility is designed and fabricated in this study. The experimental results indicate that the peak magnitude of EMP reaches up to 3210.7 kV/m and 6.02 T. The received signals depend most on the antenna and target types. The half-hohlraum generates a more intensive EMP radiation than that from the other targets, and the large planar and medium discone capture much stronger signals than the other antennas. In addition, the mechanisms of EMP generation from different targets are discussed. The resulting conclusion are expected to provide the experimental basis for further EMP shielding design.

OCIS codes: 140.3320, 140.3538, 350.5610.

doi: 10.3788/COL201614.101402.

Lasers are not only used to fabricate optical components[1,2], high-power lasers have been proposed to achieve inertial confinement fusion (ICF)[3], large laser facilities, including the Titan and NIF[4] at Lawrence Livermore National Laboratory (LLNL) in America, LMJ[5] at CEA in French, HiPER in the UK, and ShenGuang at the China Academy of Engineering Physics (CAEP), and these lasers have been developed and established. Before ICF can finally be realized, a number of fundamental issues and engineering problems need to be solved. The extremely significant electromagnetic radiation has a wide spectrum distribution (from MHz to 5 GHz) and a high-density electric field (up to MV/m), which causes malfunctions in various important diagnostics, such as x ray streak cameras and oscilloscopes[6]. In order to obtain accurate physical experimental results, it is essential to investigate the electromagnetic pulse (EMP) generation characteristics and its formation mechanism.

To measure the EMP during the process of laser shooting, researchers at the LLNL have designed some B-dots and D-dots to record the EMP signals in NIF, by which they obtained the peak magnitude of the resulting E-field signal is 167 kV/m and frequencies extending out to 5 GHz and beyond[7]. Consoli *et al.*[8] presented a dielectric electro-optic (EO) probe to measure the transient electric field, and a maximum field of 261 kV/m was measured. To interpret the mechanism of EMP generation further, Marco *et al.*[9] exposited two distinct sources of EMP emission. Tidman *et al.*[10] proposed a simple circuit model to describe the properties of the strong magnetic fields generated in laser-produced plasma. Dubois *et al.*[11] built a model of the target charging and electric field in the case of short-pulse interactions with solid targets, in which hot electrons would escape from the target surface and then created a potential drop Φ. They also found that the discharge current was related to the laser energy, pulse duration, and target size. Felber *et al.*[12] presented a model of electron currents immersed in laser plasma to explain the phenomenon of radio-frequency (RF) radiation and so on.

On the basis of preliminary study[13,14], we designed a comprehensive EMP diagnostic system and conducted a series of experiments to measure EMP signals at the ShenGuang-III laser facility. Different targets were adopted and several antennas were fabricated.

In this investigation. This experiment was carried out at the ShenGuang-III facility, which was completed in 2015[15] and which can generate complex laser pulse shapes[16]. The experimental sketch is shown in Fig. 1, where 48 ultraviolet laser beams with dimensions of 400 mm × 400 mm, pulse widths of 1–10 ns, frequency-tripled (3ω) laser energy of 180 kJ (3), and peak powers up to 600 TW were concentrated on the targets. Antenna arrays were implemented in and outside the chamber to detect the signals, as shown in Fig. 2.

Since the EMPs have broad distributions in the frequency domain, it is impossible to use one kind of antenna to measure the signals covering the entire frequency domain. Therefore, different sizes of pulsed antennas are required for collecting EMP signals in different frequency bands. Five different sets of antennas were designed as field probes. We have antennas for the electric field and

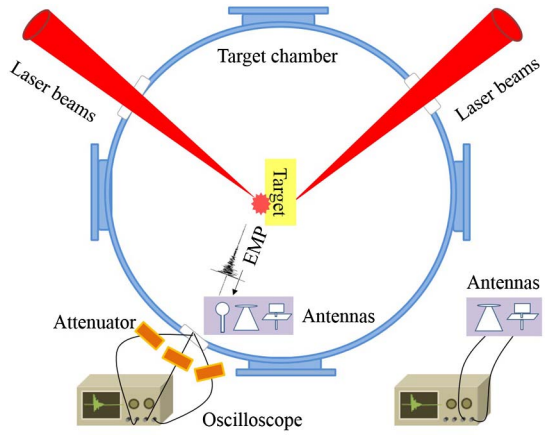

Fig. 1. Experimental sketch of the EMP diagnostics.

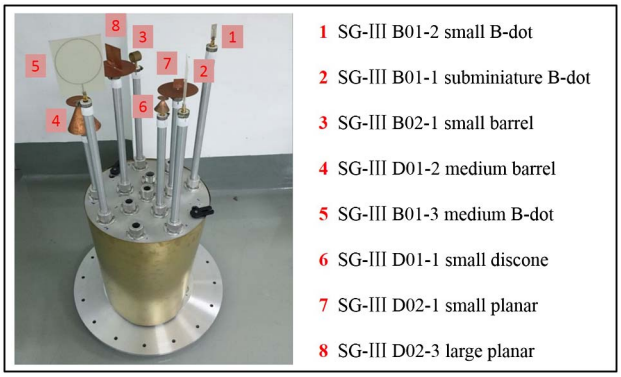

Fig. 2. Real picture of comprehensive system with antenna arrays.

magnetic field test. The electric field antennas include a discone antenna, planar antenna, and ultra-wideband dipole antenna, and the magnetic field antennas include a loop antenna (B-dot) and barrel antenna. These antennas were mounted on a flange with sticks of the same length for support and installed on the target chamber wall. The signals for each antenna were received independently. The connection between the antenna and oscilloscope was achieved using a coaxial cable inside the holder, and two oscilloscopes were used to detect the signals in real time.

In order to avoid the impact of interference on the accuracy of the signal, we designed a full-copper casing that was set between the flange and holder; it can protect the coaxial cable and shield the electromagnetic signals. In addition, suitable attenuators were used to protect the oscilloscopes in case of overloaded voltage. Some parameters are displayed in Table 1. Since all the antennas were installed in series, the distances from the antennas to the target chamber center (TCC) were different. Also, an ultra-wideband dipole antenna and a large discone antenna were installed to measure the EMP signal outside the target chamber; the distances from the target chamber wall and the TCC were 3.5 and 6.7 m, respectively, for these two antennas.

The comparisons between the laser energy and target parameters during the target shooting are given in Table 2. We selected 21 shots in this Letter, and the target types include an Au-sphere target, a flat target, a half hohlraum, a spherical vacuum hohlraum, a spherical gas-filled hohlraum, and a cylindrical gas-filled hohlraum. The Au-sphere target has a diameter of 800 μm. Disk-like flat target has a diameter of 5000 μm and Ti-film on each side that was oriented vertically. The dimensions of the half hohlraum are 1400 μm × 1000 μm. The distance from the junction of the target and the straight pipe to the laser entrance hole (LEH) was about 1000 μm. The heated half hohlraum had dimensions of 1600 μm × 1300 μm, and the LEH is face down. Two types of spherical hohlraums with the same target size of 3600 and height of 3400 μm were

Table 1. Antenna Parameters

Magnetic field antenna				
Antenna number	SGIII B01-1	SGIII B01-2	SGIII B01-3	SGIII B02-1
Antenna type	Subminiature B-dot	Small B-dot	Medium B-dot	Small barrel
Center frequency (GHz)	3.50	1.20	0.50	0.50
Distance from chamber wall (mm)	115	115	115	105

Electric field antenna						
Antenna number	SGIII D01-1	SGIII D01-2	SGIII D02-1	SGIII D02-3	SGIII D02-4	SGIII D01-3
Antenna type	Small discone	Medium discone	Small planar	Large planar	Ultra-wideband dipole	Large discone
Frequency range (GHz)	0.01–12	0.01–12	2.38–5.20	1.34–2.35	1–15	0.01–3
Distance from chamber wall (mm)	112	110	112	115	3500	3500

Table 2. Targeting Information

Shot	Target type	Target material	Focal spotsize/μm	Pulse width	Light energy of laser beams
#101201	Au-sphere	Au	500	200 ps	0.2 kJ × 16 = 3.2 kJ
#101202	Au-sphere	Au	500	200 ps	0.2 kJ × 32 = 6.4 kJ
#101203	flat	Au	500	200 ps	0.2 kJ × 32 = 6.4 kJ
#101401	Au-sphere	Au	500	200 ps	0.2 kJ × 32 = 6.4 kJ
#101402	half hohlraum	Au	500	1.2 ns	1.2 kJ × 24 = 28.8 kJ
#101901	half hohlraum	Au	500	1.0 ns	1.0 kJ × 16 = 16 kJ
#101902	half hohlraum	Au	500	1.0 ns	1.0 kJ × 16 = 16 kJ
#101903	half hohlraum	Au	500	1.0 ns	1.0 kJ × 16 = 16 kJ
#102102	half hohlraum	Au	500	1.2 ns	1.2 kJ × 24 = 28.8 kJ
#102103	half hohlraum	Au	500	1.2 ns	1.2 kJ × 24 = 28.8 kJ
#102201	half hohlraum	Au	500	1.2 ns	1.2 kJ × 24 = 28.8 kJ
#102202	half hohlraum	Au	500	3 ns	2.8 kJ × 24 = 67.2 kJ
#102602	spherical vacuum hohlraum	Au	500	3 ns	2.7 kJ × 32 = 86.4 kJ
#102701	spherical vacuum hohlraum	Au	500	3 ns	2.8 kJ × 32 = 89.6 kJ
#102801	cylindrical gas-filled hohlraum	Au	500	3 ns/3 ns	0.9 kJ × 24 + 2.8 kJ × 24 = 88.8 kJ
#110201	spherical gas-filled hohlraum	Au	500	0.5 ns/3 ns	2.8 kJ × 32 = 89.6 kJ
#110401	cylindrical gas-filled hohlraum	Au	500	0.5 ns/3 ns	0.9 kJ × 24 + 2.8 kJ × 24 = 88.8 kJ
#110501	spherical gas-filled hohlraum	Au	500	0.5 ns/3 ns	2.8 kJ × 32 = 89.6 kJ
#110601	spherical gas-filled hohlraum	Au	500	0.5 ns/3 ns	2.8 kJ × 32 = 89.6 kJ
#110602	spherical gas-filled hohlraum	Au	500	0.5 ns/3 ns	2.8 kJ × 32 = 89.6 kJ
#111101	cylindrical gas-filled hohlraum	Au	500	0.5 ns/3 ns	0.9 kJ × 24 + 2.8 kJ × 23 = 86 kJ

placed inside target chamber at the same location. A cylindrical gas-filled hohlraum had dimensions of 2400 μm × 4300 μm and was oriented vertically. The laser beams for the two gas-filled hohlraums had a pre-pulse of a 0.5 ns width and a main pulse square wave of a 3 ns width, and the waveform contrast was 1∶10.

We installed H-field antennas for the experiment, including B-dot and barrel antennas and E-field antennas for receiving signals, including a discone antenna, planar antenna, and ultra-wideband dipole antenna inside and outside the target chamber. An SMA coaxial cable was used to connect the antennas and two oscilloscopes, which output the voltage value. Figure 3 displays the voltage waveform of shot #101903. The left waveform was obtained via the 1 GHz CO10662 oscilloscope, and the right waveform was recorded by the 8 GHz MY46002309 oscilloscope. These 16 laser beams are concentrating on the half hohlraum at the same time. It can be seen that the pulse durations of the six antennas are 300, 350, 400, 150, 150, and 150 ns. The voltage amplitude signals of each antenna obtained from the same shot (#101903) were different; they had peak values of 124.1, 60.7, 1.5, 239, 456.5, and 453.5 V.

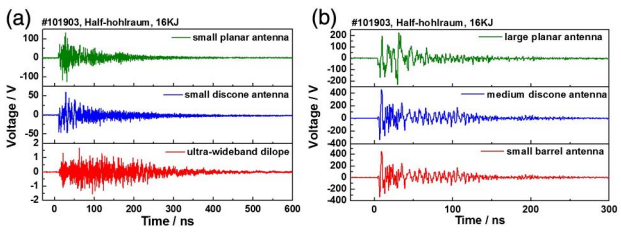

Fig. 3. Voltage signals measured from shot #101903.

The measured time-domain signals of the voltage needed to be converted to an electromagnetic field value. The methods used to process the signals from the E-field antennas and the H-field antennas were different. With regards to the electric field, the time-domain signals can be first processed through a fast Fourier transform (FFT), and then the electric field value (unit: V/m) will be obtained based on $V(\omega) = E(\omega)H(\omega)$, where $H(\omega)$ is the transfer function of the antenna. The transfer function was closely related to the gain of each antenna, with the value of gain being higher and the value of the transfer function being lower. For the H-field antenna, the magnetic field intensity (unit: T) was usually derived from the time integral on the voltage signals before it was

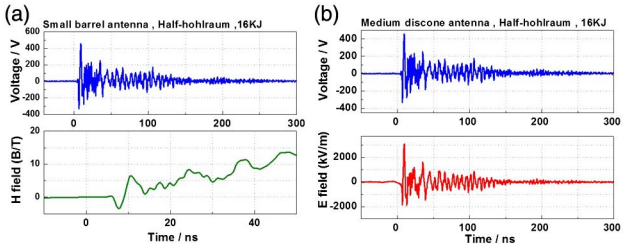

Fig. 4. EMPs measured using different antennas.

divided by the equivalent area A_{ea} (unit: mm^2). As shown in Fig. 4, the peak magnitude of the resulting magnetic field value of the small barrel antenna reached approximately 6.02 T, and the peak magnitude of the resulting electric field value of the medium discone antenna came to 3079 kV/m on the chamber wall.

There should be several factors that are able to strongly affect the EMP irradiations from laser shooting targets at the ShenGuang-III laser facility, including the laser energies, targets, and the selected antenna types. When we focused on constant target and antenna types, the E-field intensity was obtained by different E-filed antennas, as shown in Fig. 5, where the E-field intensities of Figs. 5(a)–5(f) corresponded to six kinds of targets. The peak electric fields of each target were 925, 744, 3211, 1527, 1496, and 777 kV/m. By comparing the six results, we can see that medium discone and large planar had relatively higher electric fields, but the ultra-wideband dipole showed a minimal intensity. It can also be found that peak magnitude of the electric field value was obtained at the medium discone for all targets except the Au-sphere.

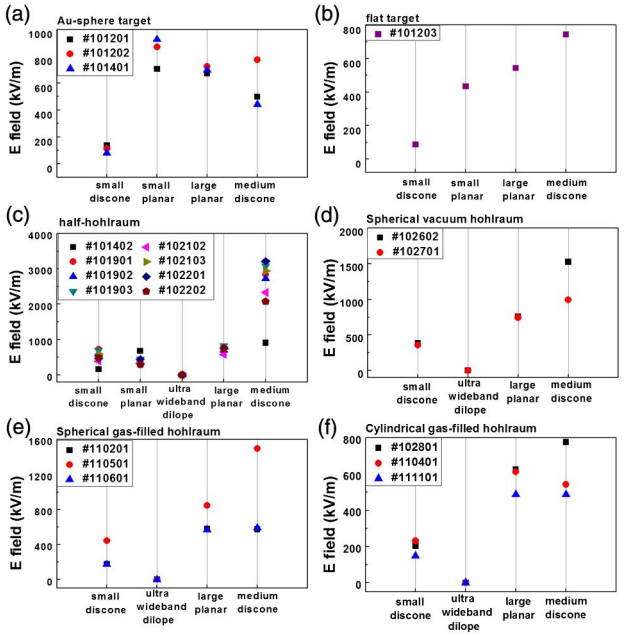

Fig. 5. Electric field intensity obtained from different antennas for six kinds of targets.

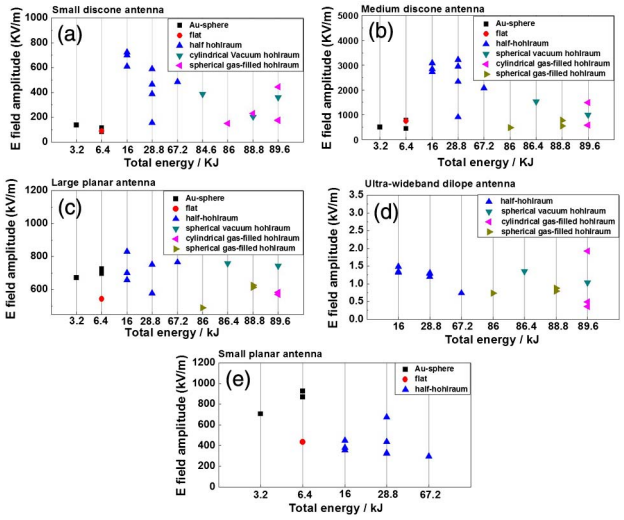

Fig. 6. Electric field intensity measured using four kinds of electric field antennas.

The E-field for each antenna was obtained when we selected a constant laser energy and an antenna type, as displayed in Fig. 6, where the E-fields of Figs. 6(a)–6(e) corresponded to five kinds of E-field antennas under different laser energies and targets. Peak magnitudes of the resulting electric field value of each antenna are 699.70, 3210.70, 845.39, 1.48, and 925 kV/m. Moreover, Fig. 7 depicts that the magnetic field intensities of the small barrel and B-dot were achieved by different laser energies and targets, and the peak magnitudes of the values were 6.02 T and 0.25 mT, separately. The comparisons of the six figures confirmed that the peak magnitude of the electric field or magnetic field value could be obtained at the half-hohlraum target for all antennas except for the small planar.

The different gain and efficiency of each antenna contributed to the alteration of the voltage, which was also related to the varying frequency band of each antenna. Figure 5 indicates that the large planar and medium discone antennas obtained the strongest EMP signals compared with the other antennas, which can be attributed to the better omnidirectional ability to receive signals of these two antennas and also because the high electric field value resulted from the inverse relationship between the transform function and gain, with the large planar having a low gain but a high voltage value. Moreover, the medium discone possessed a wider frequency band

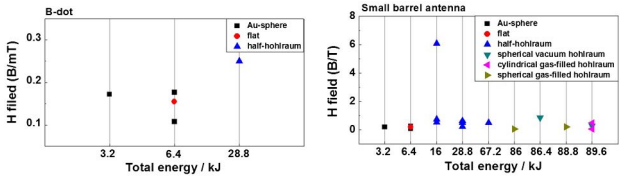

Fig. 7. Magnetic field intensity measured using small barrel antenna and B-dot.

(0.01–12 GHz). In contrast, the ultra-wideband dipole antenna was installed outside the target chamber and remained far away from TCC, so it could only get a low electric field value.

To sum up the above electric field results from the different targets, the highest electric field value was obtained when the laser with the highest power interacted with the half hohlraum, which was mainly because the half hohlraum had a semi-closed shape and the laser repeatedly irradiated the target, meaning laser could couple to the golden cavity wall many times. Also, the half hohlraum had a smaller solid angle than the flat target, so the hohlraum could more effectively collect the laser beams. Most of data demonstrated that the vacuum hohlraum had a better capacity to generate EMPs than the gas-filled hohlraum. Usually, the low-Z gas fills in the hohlraum could control the motion of the plasma on the cavity wall, which reduced both the blocking effects and the laser energy damping along the lightpath to ensure the effective absorption of the laser on the wall. However, the intensity of the scattered light generated by the laser-plasma interaction in the gas-filled hohlraum was stronger than the vacuum hohlraum, which tended to reduce the energy absorption and lower the laser-plasma coupling productivity directly[17]. In addition, different laser power densities also led to the variation of the EMP signals; a low power density is more conducive to implosion.

Simulations about the coupling of the laser and the flat target could be found in some Letters[10,18,19]. During the interaction of the laser pulses with the flat target in the case of oblique incidence, circular spontaneous magnetic fields were produced, with electrons going away from the target, and electrostatic fields were forming behind the target at the same time. It was also confirmed by the electrons from the ultra-laser interactions with the cylindrical hohlraum using the particle-in-cell method[20]. The strong laser interacted with the hohlraum wall at the entrance, which can produce a large number of super-hot electrons through the mechanism of $J \times B$ heating and vacuum heating. When the ultra-laser incidents on the hohlraum, hot electrons are ejected from the side wall and generate a quasi-static charge separation field E_s simultaneously. Surface current I_s was formed when a large number of hot electrons propagated alone the target surface, and the return current I_r was formed when cold electrons returned back to the target. These two currents composed a circular electric current together, and then a quasi-static magnetic field was generated. In the repeated process of super-hot electrons escaping and refluxing, the different energies that the super-hot electrons carried led to different frequencies of the EMP signal.

Some reports indicated that EMP field could be higher, nearer to the TCC[21], and the power of the EMP was proportional to $1/r^2$, where r was the distance from the antenna to the TCC. We had already measured high-level (on the order of MV/m) and broad-spectrum EMP signals on the target chamber wall, and it was speculated that more intense EMP signals existed at the center of the chamber.

In this Letter, we adopt a suite of self-designed antennas to collect EMP signals, and different types of targets are selected to receive laser irradiation. The peak magnitude of the electric field is up to the order of MV/m, and the magnetic field is up to 6.02 T. The half hohlraum generates higher EMP signals than the other targets. The large planar and medium discone receive a stronger signal than the other antennas. Most of the experimental results show intense electromagnetic interference generated by the coupling of the laser and the target inside and outside the target chamber, so it is necessary to make the proper electromagnetic shield. The generation mechanism of the EMP signals for different targets is discussed but still needs to be investigated and determined. In our future work, the specific shielding design of EM interference will be put forward for all kinds of diagnostic equipment at the Shen-Guang-III laser facility.

This work was financially supported by the Fundamental Research Funds for the Central Universities (No. ZYGX2015J108) and the National Natural Science Foundation of China (Nos. 11575166 and 51581140). M. Yang's e-mail address is 15102885415@163.com.

References

1. X. Tan, L. Jiang, J. Hu, P. Liu, A. Wang, and Y. Lu, Chin. Opt. Lett. **13**, 111401 (2015).
2. B. Gao, T. Chen, V. Khuat, J. Si, and X. Hou, Chin. Opt. Lett. **14**, 021407 (2016).
3. X. G. Basov, P. G. Kriukov, S. D. Zskhrrov, Y. V. Senatsky, and S. V. Tchekalin, IEEE J. Quantum Electron. **4**, 864 (1968).
4. C. A. Haynam, P. J. Wegner, J. M. Auerbach, M. W. Bowers, S. N. Dixit, G. V. Erbert, G. M. Heestand, M. A. Henesian, M. R. Hermann, K. S. Jancaitis, K. R. Manes, C. D. Marshall, N. C. Mehta, J. Menapace, E. Moses, J. R. Murray, M. C. Nostrand, C. D. Orth, R. Patterson, R. A. Sacks, M. J. Shaw, M. Spaeth, S. B. Sutton, W. H. Williams, C. C. Widmayer, R. K. White, S. T. Yang, and B. M. V. Wonterghem, Appl. Opt. **46**, 3276 (2007).
5. C. Cavailler, Plasma Phys. Controlled Fusion **47**, B389 (2005).
6. C. G. Brown, M. J. Ayers, B. Felker, W. Ferguson, J. P. Holder, S. R. Nagel, K. W. Piston, N. Simanovskaia, A. L. Throop, M. Chung, and T. Hilsabeck, Rev. Sci. **83**, 100729 (2012).
7. D. C. Eder, A. Throop, C. G. Brown, and J. Kimbrough Jr., Lawrence Livermore National Laboratory Report LLNL-TR-411183 (2009).
8. F. Consoli, R. De Angelis, L. Duvillaret, P. L. Andreoli, M. Cipriani, G. Cristofari, G. Di Giorgio, F. Ingenito, and C. Verona, Sci. Rep. **6**, 27889 (2016).
9. M. De Marco, J. Cikhardt, J. Krása, A. Velyhan, M. Pfeifer, E. Krouský, D. Klír, K. Řezáč, J. Limpouch, D. Margarone, and J. Ullschmied, Nukleonika **60**, 239 (2015).
10. D. A. Tidman, Appl. Phys. Lett. **22**, 498 (1973).
11. J. L. Dubois, F. Lubrano-Lavaderci, D. Raffestin, J. Ribolzi, J. Gazave, A. Compant La Fontaine, E. d'Humieres, S. Hulin, P. Nicolai, A. Poye, and V. T. Tikhonchuk, Phys. Rev. E Stat. Nonlin. Soft Matter Phys. **89**, 013102 (2014).
12. F. S. Felber, Appl. Phys. Lett. **86**, 231501 (2005).

13. J. Yang, T. Yi, T. Li, C. Wang, R. Wang, Z. Gao, S. Liu, Y. Ding, and S. Jiang, High Power Laser Part. Beams **27**, 41013 (2015).
14. M. Yang,, T. Yi, J. Yang, C. Wang, T. Li, S. Liu, S. Jiang, and Y. Ding, Chin. J. Lasers **43**, 0801009 (2016).
15. W. Zheng, X. Wei, Q. Zhu, F. Jing, D. Hu, J. Su, K. Zheng, X. Yuan, H. Zhou, W. Dai, W. Zhou, F. Wang, D. Xu, X. Xie, B. Feng, Z. Peng, L. Guo, Y. Chen, X. Zhang, L. Liu, D. Lin, Z. Dang, Y. Xiang, and X. Deng, High Power Laser Science Eng. **4**, e21 (2016).
16. D. Hu, J. Dong, D. Xu, X. Huang, W. Zhou, X. Tian, D. Zhou, H. Guo, W. Zhong, X. Deng, Q. Zhu, and W. Zheng, Chin. Opt. Lett. **13**, 041406 (2015).
17. H. Wei, D. Yang, T. Xu, F. Wang, and X. Peng, High Power Laser Part. Beams **26**, 032006 (2014).
18. H. Schwoerer, S. Pfotenhauer, O. Jackel, K. U. Amthor, B. Liesfeld, W. Ziegler, R. Sauerbrey, K. W. Ledingham, and T. Esirkepov, Nature **439**, 445 (2006).
19. A. Poye, J. L. Dubois, F. Lubrano-Lavaderci, E. D'Humieres, M. Bardon, S. Hulin, M. Bailly-Grandvaux, J. Ribolzi, D. Raffestin, J. J. Santos, P. Nicolai, and V. Tikhonchuk, Phys. Rev. E Stat. Nonlin. Soft Matter Phys. **92**, 043107 (2015).
20. W. He, W. Zhou, Z. Zhang, J. Jiao, L. Shan, and G. Jiang, High Power Laser Part. Beams **27**, 072003 (2015).
21. C. G. Brown, T. J. Clancy, D. C. Eder, W. Ferguson, and A. L. Throop, EPJ Web Conf. **59**, 08012 (2013).